




<b>Publication Year</b>	2021
<b>Acceptance in OA @INAF</b>	2022-06-09T14:48:14Z
<b>Title</b>	Dorado and its member galaxies II: A UVIT picture of the NGC 1533 substructure
<b>Authors</b>	RAMPAZZO, Roberto; MAZZEI, Paola; Marino, A.; Bianchi, L.; Ciroi, S.; et al.
<b>DOI</b>	10.1007/s12036-021-09690-x
<b>Handle</b>	<a href="http://hdl.handle.net/20.500.12386/32252">http://hdl.handle.net/20.500.12386/32252</a>
<b>Journal</b>	JOURNAL OF ASTROPHYSICS AND ASTRONOMY
<b>Number</b>	42



## SCIENCE RESULTS

# Dorado and its member galaxies II: A UVIT picture of the NGC 1533 substructure

R. RAMPAZZO<sup>1,2,\*</sup> , P. MAZZEI<sup>2</sup>, A. MARINO<sup>2</sup>, L. BIANCHI<sup>3</sup>, S. CIROI<sup>4</sup>,  
E. V. HELD<sup>2</sup>, E. IODICE<sup>5</sup>, J. POSTMA<sup>6</sup>, E. RYAN-WEBER<sup>7</sup>, M. SPAVONE<sup>5</sup>  
and M. USLENGHI<sup>8</sup>

<sup>1</sup>INAF Osservatorio Astrofisico di Asiago, Via Osservatorio 8, 36012 Asiago, Italy.

<sup>2</sup>INAF Osservatorio Astronomico di Padova, Vicolo dell'Osservatorio 5, 35122 Padua, Italy.

<sup>3</sup>Department of Physics and Astronomy, The Johns Hopkins University, 3400 N. Charles St., Baltimore, MD 21218, USA.

<sup>4</sup>Department of Physics and Astronomy, University of Padova, Vicolo dell'Osservatorio 3, 35122 Padua, Italy.

<sup>5</sup>INAF-Osservatorio Astronomico di Capodimonte, Salita Moiariello 16, 80131 Naples, Italy.

<sup>6</sup>University of Calgary, 2500 University Drive NW, Calgary, Alberta, Canada.

<sup>7</sup>Centre for Astrophysics and Supercomputing, Swinburne University of Technology, Hawthorn, VIC 3122, Australia.

<sup>8</sup>INAF-IASF, Via A. Curti, 12, 20133 Milan, Italy.

\*Corresponding Author. E-mail: roberto.rampazzo@inaf.it

MS received 30 October 2020; accepted 17 December 2020

**Abstract.** Dorado is a nearby (17.69 Mpc) strongly evolving galaxy group in the Southern Hemisphere. We are investigating the star formation in this group. This paper provides a FUV imaging of NGC 1533, IC 2038 and IC 2039, which form a substructure, south west of the Dorado group barycentre. FUV CaF2-1 UVIT-Astrosat images enrich our knowledge of the system provided by GALEX. In conjunction with deep optical wide-field, narrow-band H $\alpha$  and 21-cm radio images we search for signatures of the interaction mechanisms looking in the FUV morphologies and derive the star formation rate. The shape of the FUV luminosity profile suggests the presence of a disk in all three galaxies. FUV emission is detected out to the optical size for IC 2038, and in compact structures corresponding to H $\alpha$  and H II bright features in NGC 1533. A faint FUV emission, without an optical counterpart, reminiscent of the H I structure that surrounds the outskirts of NGC 1533 and extends up to IC 2038/2039, is revealed above the local background noise.

**Keywords.** Ultraviolet: galaxies—galaxies: elliptical and lenticular—cD—galaxies: spiral—galaxies: interaction—galaxies: evolution..

## 1. Introduction

One of the breakthrough provided by the *Galaxy Evolution Explorer* (GALEX hereafter) (Martin *et al.* 2005; Morrissey *et al.* 2007) is the direct evidence of galaxy transformation in groups. UV-optical colour magnitude diagrams (CMDs hereafter) highlighted an

intermediate region, the green valley, populated by transforming galaxies (see e.g. Salim *et al.* 2007; Schawinski *et al.* 2007) located between the sequence of red galaxies, mostly evolved early-type (Es+S0-s = ETGs hereafter), and the blue cloud composed of late-type (LTGs hereafter), star forming galaxies. Ranking groups according to their blue vs. red sequence and green valley galaxy populations, UV-optical CMDs contribute to correlate the group structure, kinematics and dynamics to its members

This article is part of the Special Issue on “AstroSat: Five Years in Orbit”.

evolutionary phase. Marino *et al.* (2010, Marino *et al.* 2013) investigated loose groups, rich of LTGs, analogs of our Local Group. This kind of groups lack a well defined red sequence. At odd, less dispersed groups with an increasing fraction of ETGs start to develop a galaxy population inhabiting both the red sequence and the green valley. Very rich groups, in an advanced stage of virialization, like NGC 5486 group, the third richest association in the nearby universe after Virgo and Fornax, show a well developed red sequence and a still rich green valley (Marino *et al.* 2016; Mazzei *et al.* 2014b, 2019 and references therein). The enrichment of the red sequence and of the green valley traces the transition from loose yet un-virialized groups to rich, more compact and virialized ones (see e.g. Rampazzo *et al.* 2018).

Driven by the gravitational force, that collapses groups and makes galaxies to interact, mechanisms leading to a galaxy morphological metamorphosis can either quench or re-ignite the star formation (SF). Mechanisms involved are of several types and seem to depend on the environment density (see e.g. Boselli & Gavazzi 2006, 2014). Mergers can transform spirals into ellipticals and S0s (see e.g. Toomre & Toomre 1972; Barnes 2002; Mazzei *et al.* 2014a and references therein) and quench SF by ejecting the interstellar medium via supernovæ, AGN or shock-driven winds (see e.g. Di Matteo 2015 and references therein). Ram-pressure, that may strip the gas reservoirs is supposed to work mostly in rich environments (Boselli & Gavazzi 2014; Ramatsoku *et al.* 2019), but there are evidences (e.g. in H I) that it also works for groups (Bureau & Carignan 2002; Kantharia *et al.* 2005). There are examples of mass-transfer between gas-rich and gas-poor companion galaxies, e.g. physical pairs composed of a LTG and an ETGs, that may re-fuel SF (see e.g. Domingue *et al.* 2003; Keel 2004; Chung *et al.* 2006; Plana *et al.* 2017a, b).

In this paper, we focus on the nearby Dorado group in the Southern Hemisphere (RA = 64.3718 [deg], Dec = -55.7811 [deg]) as defined by Kourkchi and Tully (2017) (see also, Firth *et al.* 2006 and references therein). Throughout the paper, we adopt 17.69 Mpc as the distance of all Dorado candidate members. Dorado CMD is described in Fig. 1 of Cattapan *et al.* (2019). The red sequence of the group includes several ETGs. A set of intermediate luminosity member galaxies is still crossing the green valley. Basically only NGC 1566, a bright grand design spiral, is still located in the blue cloud. With respect to evolved groups (e.g. NGC 5486, see Marino *et al.* 2016) Dorado seems to be in an earlier and active

evolutionary phase. Several indications support this view like the group clumpy structure. A compact group, SGC 0414-5559 (Iovino 2002) is located at the barycentre of the group as defined by Kourkchi & Tully (2017). The compact group is dominated by two ETGs, NGC 1549 an E and NGC 1553 an S0, both showing a wide shell structure. The Dorado group members morphology shows indeed the nearly ubiquitous presence of interaction signatures such as shells, asymmetries, tails (see e.g. Malin & Carter 1983; Cattapan *et al.* 2019). Star-forming rings have been also revealed in several ETGs (Rampazzo *et al.* 2020). Dorado is an atomic gas rich group. Nearly half of the entire H I content of the Dorado group,  $3.5 \times 10^{10} M_{\odot}$ , is located in the spiral member NGC 1566, although H I has been also detected in several other members, independently from their morphological classification (Kilborn *et al.* 2005, 2009). Rampazzo *et al.* (2020), presented their H $\alpha$ + [N II] study aiming at investigating the star formation rate (SFR hereafter) of the Dorado backbone galaxies. They found that SFR in LTGs is fading while in ETGs is not yet shut-down. Rampazzo *et al.* (2020) suggested that mechanisms such as gas stripping and gas accretion, through galaxy-galaxy interaction, seem relevant in the evolutionary phase of Dorado.

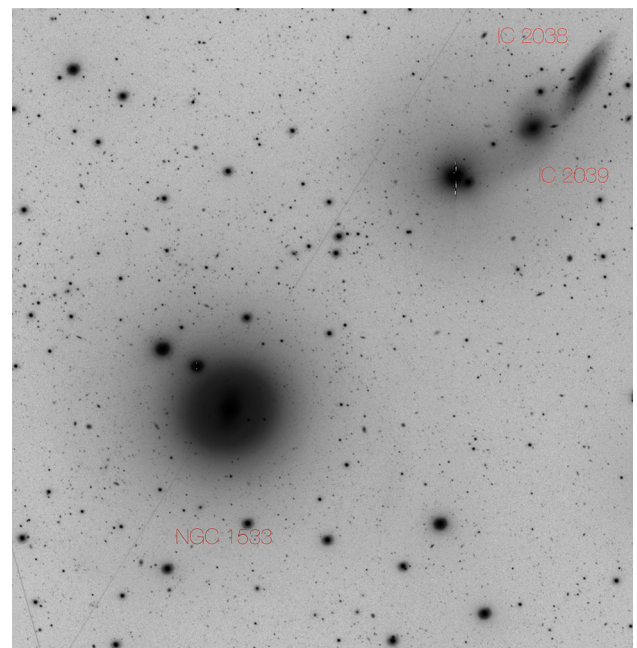


**Figure 1.** NGC 1533 sub-structure. VST deep image in the SDSS *g*-band of the IC 2038, IC 2039 (north west side) and NGC 1533 (south east side). The image size is  $14' \times 14.7'$ . Astrosat-UVIT observations (see Table 1), cover the entire sub-structure.

This work complements the Rampazzo *et al.* (2020) study, using FUV CaF2-1 (1300–1800 Å) broad filter (similar to *GALEX* FUV; see Tandon *et al.* 2017) observations obtained with Astrosat-UVIT of the Dorado members. The UVIT targets partly cover the galaxy set observed in H $\alpha$ + [N II] by Rampazzo *et al.* (2020). In this paper, we investigate the sub-structure, SW of the Dorado barycentre, formed by NGC 1533, IC 2038 and IC 2039. Our goal is to analyze the FUV morphological structure of galaxies in this sub-structure and the relation between H $\alpha$  regions and the FUV emission. H $\alpha$  emission has been found not only in the Scd galaxy IC 2038 but also in the E-S0 galaxy NGC 1533 (Rampazzo *et al.* 2020).

The paper plan is the following. In Section 2, we summarize our knowledge about the NGC 1533 sub-structure. UVIT observations and the reduction are presented in Section 3. In Section 4, the photometric analysis and the comparison with *GALEX* observations are presented. The results are given in Section 5 and discussion is presented in Section 6. Section 7 contains summary and conclusion.

## 2. NGC 1533 substructure and the Dorado group

According to Kourkchi and Tully (2017), Dorado has an average redshift of  $1230 \pm 89 \text{ km s}^{-1}$  and a velocity dispersion of  $242 \text{ km s}^{-1}$ . NGC 1533 and the pair IC 2038/39 form a sub-structure of the group with an average redshift of  $764 \pm 43 \text{ km s}^{-1}$  (see Table 1). Figure 1 shows a deep image of the NGC 1533 sub-structure in the SDSS *g*-band ( $\mu_g \approx 30 \text{ mag arcsec}^{-2}$ ) obtained within the *VST Early-type Galaxy Survey (VEGAS<sup>1</sup>)* (see e.g. Capaccioli *et al.* 2015). This sub-structure is located at the south west periphery of Dorado group barycentre formed by the SCG 0414-5559 compact group, well separated, both in radial velocity and in projection, from other member candidates.

NGC 1533 has been investigated with *GALEX* by Marino *et al.* (2011a, b). Rampazzo *et al.* (2017) investigated this galaxy with *Swift*. All these studies evidenced an outer FUV bright ring. In correspondence to the FUV ring, Rampazzo *et al.* (2020) found some H $\alpha$  complexes. Moreover they found that while the SFR is enhanced in NGC 1533 it is depressed in IC 2038, if compared with the general sample of ETGs (Gavazzi *et al.* 2018) and of Spirals (James *et al.* 2004), respectively. Rampazzo *et al.* (2020) found

that in IC 2038 H II regions are distributed along the galaxy body, which appears slightly elongated towards the companion galaxy, IC 2039, in the SE direction.

More recently, deep optical observations, in *g* and *r* bands, of NGC 1533 and IC 2038/39 have been analysed by Cattapan *et al.* (2019) using the VLT Survey Telescope (VST) at the European Southern Observatory, Chile. They evidenced a large disk around NGC 1533 and several tails suggesting that NGC 1533 and the nearby pair are evolving together (Cattapan *et al.* 2019).

The NGC 1533 Dorado substructure has been mapped in H I by Ryan-Weber *et al.* (2004) (see also Kilborn *et al.* 2005, 2009) showing and extended H I structure that extends from 1533 up to IC 2038/39 pair. Werk *et al.* (2008, 2010) reported that there are some star forming regions well outside NGC 1533 with the same radial velocity as the H I gas revealed by Ryan-Weber *et al.* (2004; see their Fig. 7 for J0409-56). The narrow-band H $\alpha$ + [N II] study by Rampazzo *et al.* (2020) detected three H $\alpha$  regions in correspondence of the regions detected by Werk *et al.* (2010) confirming that such outer H II regions belong to NGC 1533 sub-structure.

In this context, the study of the NGC 1533 sub-structure is relevant both for the general understanding of the evolution of gas-rich merging events and for the study of local SF mechanisms.

## 3. Observations and reduction

Astrosat is a multi-wavelength satellite that has been launched by the Indian Space Research Organization on September 28, 2015. The ultraviolet-optical telescope on board is the Ultra-Violet Imaging Telescope facility UVIT (Tandon *et al.* 2017). It is composed of two Ritchey-Chretien telescopes with 37.5-cm aperture, a circular field-of-view of 28' diameter, observing simultaneously one in FUV (1300–1800 Å) and the other both in NUV (2000–3000 Å) and optical band, VIS (3200–5500 Å), by means of a beam-splitter directing NUV and VIS to individual cameras.

Since the NUV channel was not operative during our runs, observations have been performed with the FUV channel only. We used the full field-of-view, in photon counting mode with the Filter F148W CaF<sub>2</sub> ( $\lambda_{\text{mean}} = 1481, \Delta\lambda = 500 \text{ Å}$ ). Photons are counted on a planar CMOS array at approximately 28 Hz and stacked on the ground with shift and add algorithms (for details, see Kumar *et al.* 2012; Postma *et al.*

<sup>1</sup>Visit the website <http://www.na.astro.it/vegas/VEGAS/Welcome.html>.

**Table 1.** Relevant properties of members of Dorado in the UVIT FoV from the literature.

Field centre	ID source	RA (J2000)	Dec. (J2000)	FUV (mag)	$V_{\text{hel}}$ (km s <sup>-1</sup> )	Morpho. type
A	IC 2038	04 08 53.76	-55 59 22.2	17.25 ± 0.02*	712	7.0
	IC 2039	04 09 02.37	-56 00 42.1	19.98 ± 0.07*	817	-3.1
B	NGC 1533	04 09 51.84	-56 07 06.6	16.90 ± 0.02 <sup>†</sup>	764	-2.5

Column 1: UVIT field. Column 2: Source identification. Columns 3 and 4 provide right ascension and declination of the sources. Column 5 lists the FUV total integrated magnitudes from *GALEX* archive (indicated with an \*) and reported in NED (indicated with <sup>†</sup>). Columns 6 and 7 report the heliocentric radial velocity and the galaxy morphological type, respectively, from Kourkchi and Tully (2017).

2011; Postma & Leahy 2017; Tandon *et al.* 2017) with the astrometric world coordinate solution solved automatically by a trigonometric algorithm (Postma & Leahy 2020).

Table 2 reports the relevant characteristics of our UVIT observations. Astrosat-UVIT observations are the result of the proposal A07\_010 (PI R. Rampazzo) and cover the south west part of Dorado, in particular Astrosat-UVIT fields contain IC 2038 and IC 2039 (Field A) and NGC 1533 (Field B).

#### 4. Data analysis and comparison with the literature

In this section, we present the data analysis performed and the comparison with the current literature mainly from *GALEX* study. Original images with 0".416 per sub-pixel have been rebinned 4 × 4 providing a final scale of 1".664 px<sup>-1</sup>.

##### 4.1 Integrated FUV magnitudes

Column 3 of Table 3 provides the FUCaF2-1, UVIT integrated magnitudes. In Fig. 2, we compared our results with integrated magnitudes reported in Table 1 from *GALEX* observations. The figure shows the good agreement between our values and those in the current literature.

##### 4.2 Surface photometry

The surface photometry is obtained using the IRAF task ELLIPSE (Jedrzejewski 1987). In obtaining the surface brightness profile, ELLIPSE accounts for the geometrical information contained in the isophotes and allows the variation of the ellipticity,  $\epsilon = (1 -$

$b/a)$  and of the position angle, ( $PA$ ), along the ellipse major axis ( $a$ ). In addition, ELLIPSE provides measure of the isophotal shape parameter, the so-called  $a_4$  parameter from the fourth cosine component of the Fourier analysis of the fitted ellipse, allowing to distinguish between boxy ( $a_4 < 0$ ) and discy ( $a_4 > 0$ ) isophotes (Bender *et al.* 1988). This approach, widely used with optical images of ETGs, has been adopted to investigate *GALEX* FUV data by Jeong *et al.* (2009) and Marino *et al.* (2011b). FUV geometric profiles have not been provided by the above papers.

In fitting isophotes we allowed  $\epsilon$ , and  $PA$  to vary with the galacto-centric distance, in order to obtain a good description of the FUV luminosity distribution. Our FUV images either show irregular peculiar features (NGC 1533), clumpy and spiral features (IC 2038) or have a low signal-to-noise (IC 2039). This is the reason for which we provide in Table 3 only the average ellipticity,  $\langle \epsilon \rangle$  and position angle,  $\langle PA \rangle$ , (columns 4 and 5 respectively) of the galaxy. In presence of irregular, peculiar features, sudden variations in both  $\epsilon$  and  $PA$  are expected and, in particular, the isophotal shape parameter,  $a_4$ , loses its physical meaning.

The pair IC 2038/IC 2039 has not been previously investigated with *GALEX*. Marino *et al.* (2011b) obtained the surface brightness profiles NGC 1533. Figure 3 shows the comparison between the Marino *et al.* (2011b) and our luminosity profile. The luminosity profiles compare quite well outside 30", suggesting that there is a very small, if any, zero point effect, while the central region differs significantly. The reason of such a difference in the central part is not entirely clear, although in FUV the *GALEX* PSF FWHM is 4.2" with respect to 1.5" of UVIT (see Morrissey *et al.* 2007; Tandon *et al.* 2017, 2020). Substructures on spatial scales (projected on the sky)  $\lesssim 0.4$  kpc are washed out in the *GALEX* profile, but are picked up in the UVIT data. In particular, the FUV

**Table 2.** UVIT observations.

Field ID	Obs ID	Observing date (s)	Exp. time	Target ID
A	A07_010T04_9000003220	October 5, 2019	6481.278	IC 2038
B	A07_010T05_9000003236	October 16, 2019	6628.734	NGC 1533

Field identification in column 2 refers to the proposal A07\_010 (PI. R. Rampazzo). Column 3 and column 4 report the observing date and the total reduced exposure time. In column 5, the central target is quoted. The nominal zero point magnitude of the FUV channel and the physical plate scale are 18.08 mag and 3''/33 respectively, as reported in Tandon *et al.* (2017).

**Table 3.** Relevant FUV parameters of galaxies in the NGC 1553 sub-structure.

Field	ID source	FUV (mag)	$\langle\epsilon\rangle$	$\langle PA\rangle$ (°)	$n$	$L_{\text{FUV}}$ (erg s <sup>-1</sup> Hz <sup>-1</sup> )	SFR ( $M_{\odot}$ yr <sup>-1</sup> )
A	IC 2038	17.19 ± 0.07	0.72 ± 0.02	154.4 ± 4.6	0.81 ± 0.09	1.81 × 10 <sup>27</sup>	0.025 ± 0.002
	IC 2039	20.03 ± 0.11	0.19 ± 0.05	104.1 ± 8.7	1.45 ± 0.18	1.33 × 10 <sup>25</sup>	0.002 ± 0.0002
B	NGC 1533	16.74 ± 0.15	...	...	2.64 ± 0.06	2.74 × 10 <sup>26</sup>	0.038 ± 0.006

Column 1: UVIT field. Column 2: Source identification; column 3: FUV integrated magnitude corrected for galactic extinction accounting for  $A_{\text{FUV}} = 7.9 \times E(B - V)$ ;  $E(B - V)$  is 0.01 mag both for IC 2038 and IC 2039, 0.015 mag for NGC 1533 from NED. Luminosities are computed accounting for the same distance, 17.69 Mpc, for all our targets. In columns 4 and 5, the average ellipticity and position angles are provided: for NGC 1533, see Section 5. In column 6, the Sérsic index from the best-fit of the entire profile is reported. In columns 7 and 8, the FUV luminosity and the SFR computed according to the Lee *et al.* (2009) provided in Section 6.3, are reported.

knot that peaks at  $\approx 25''$  (indicated as A in Fig. 5) is clearly smoothed out in Marino *et al.* (2011b), suggesting a significant role played by the PSF in driving the *GALEX* surface photometry.

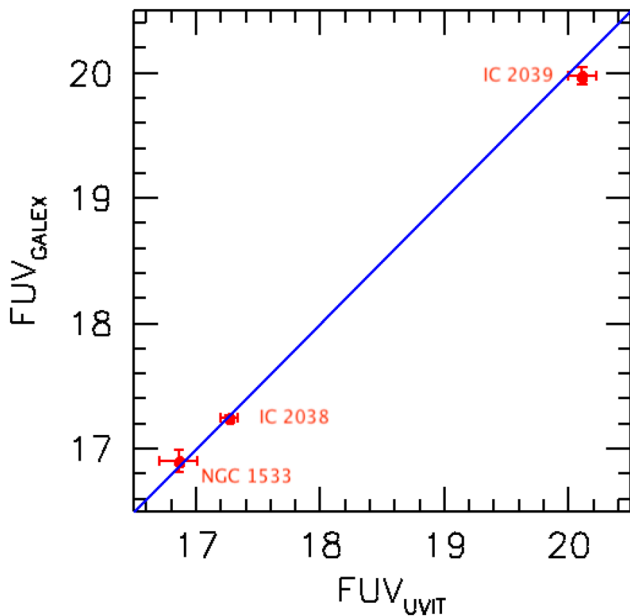


**Figure 2.** Comparison between UVIT FUV CaF<sub>2</sub>-1 integrated magnitudes of Dorado members with those from *GALEX* available in the literature. Magnitudes in the plot are not corrected for galactic extinction.

Figures 4 and 5 show the FUV image and the luminosity profile of the pair members IC 2038/39 and of NGC 1533, respectively. The bottom panel of these figures shows a color composite RGB image of the galaxies obtained from the present FUV image, the continuum and H $\alpha$ +[N II] images from Rampazzo *et al.* (2020).

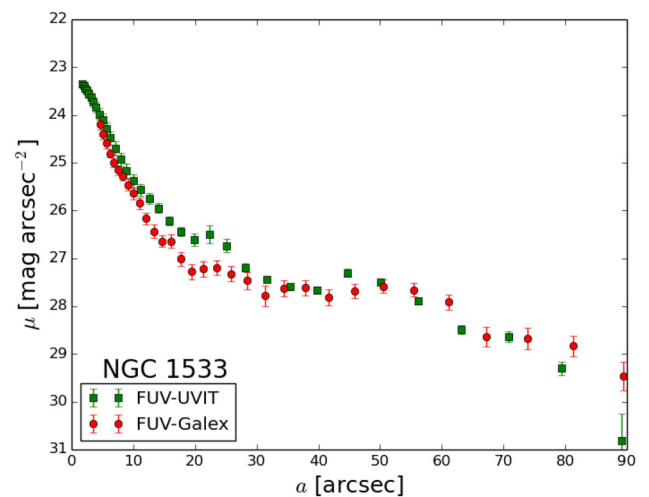


**Figure 3.** Comparison of the present FUV luminosity profile of NGC 1533 with Marino *et al.* (2011b) from *GALEX* pointed observations.

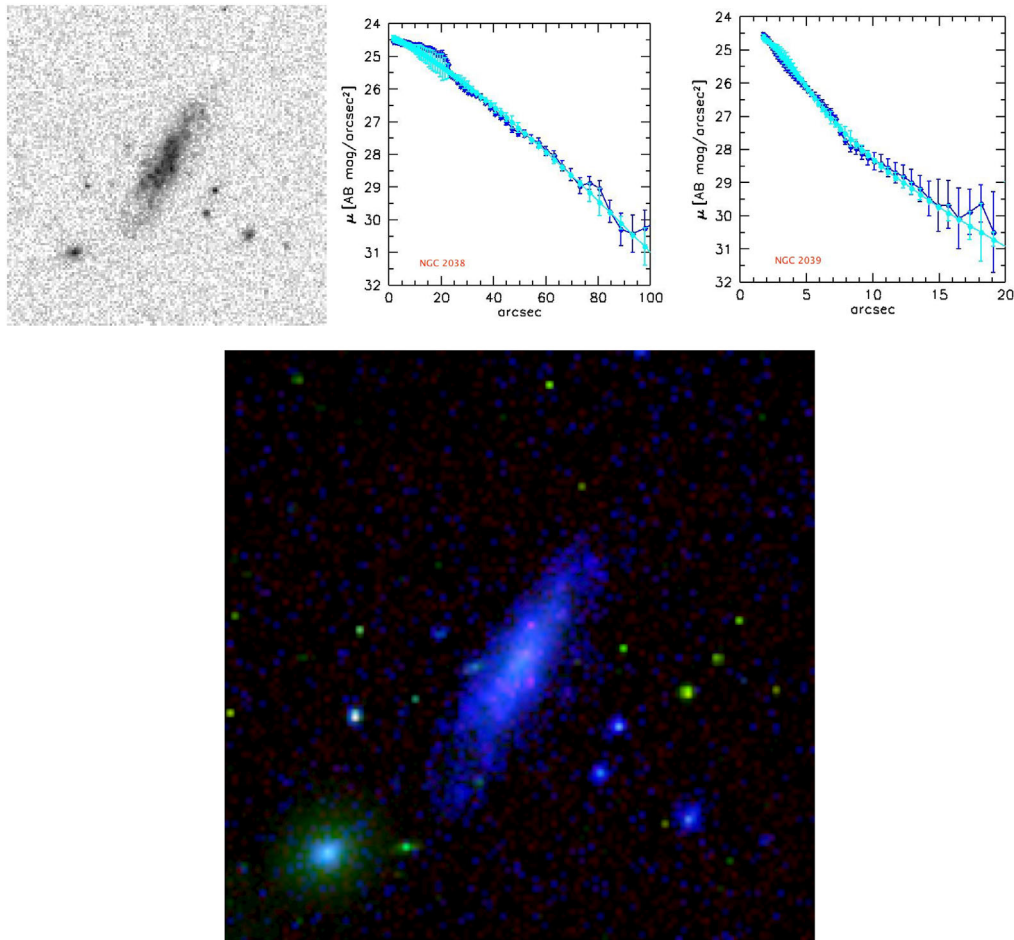


**Figure 4.** (Top: left panel) FUV image of IC 2038 (Sbc) and of IC 2039 (E), its physical companion, in the south east. The image size is  $4' \times 4'$ . North on the top, east to the left. (Top: mid and right panels) FUV surface brightness profile of IC 2038 and of IC 2039 (blue dots). Single Sérsic law fit of the luminosity profiles, discussed in Section 5 are also shown as cyan dots. The values of the Sérsic index are  $n = 0.81 \pm 0.09$  and  $n = 1.45 \pm 0.18$ , for IC 2038 and IC 2039, respectively. (Bottom panel) Color-composite RGB image using the red and the green channels for H $\alpha$  and the nearby continuum (Rampazzo *et al.* 2020) and the blue channel for the FUV image. Both the H $\alpha$  and the continuum PSF have been re-scaled to the PSF of the FUV image.

### 4.3 Luminosity profile fitting

We fit the shape of the FUV luminosity profile with a Sérsic law (Sérsic 1963). Even a crude representation of the light profile, as a simple Sérsic law fit, provides useful information, and sometimes is the only decomposition that can be compared with the literature. The Sérsic law  $\mu \propto r^{1/n}$ , where  $\mu$  is the surface brightness and  $r$  the radius, is a generalization of the de Vaucouleurs (1953)  $r^{1/4}$  and of the Freeman (1970) exponential laws. The variation of the Sérsic index,  $n$ , describes the manifold of the shapes of luminosity profiles of ETGs. The watershed can be considered the value  $n = 4$  representing a

‘classic’ elliptical. A classic exponential disc (Freeman 1970) in S0s has an index  $n = 1$ .

FUV luminosity profiles of ETGs may reach large values of  $n$  (see e.g. Marino *et al.* 2011b). Rampazzo *et al.* (2017) suggested that in luminosity profiles with  $n < 3$  the presence of a disc starts to emerge.

The Sérsic law fit is shown in the right panel/s of Figs. 4 and 5 for IC 2038/IC 2039 and NGC 1533, respectively, superposed to the luminosity profile. The fit is extended to the entire profile without masking FUV bright sub-structures such as the ring (B) and the knot (A) in NGC 1533. The Sérsic fit accounts for the UVIT-PSF so it is not necessary to avoid the inner part of the luminosity profile certainly ‘contaminated’ by the instrument PSF.

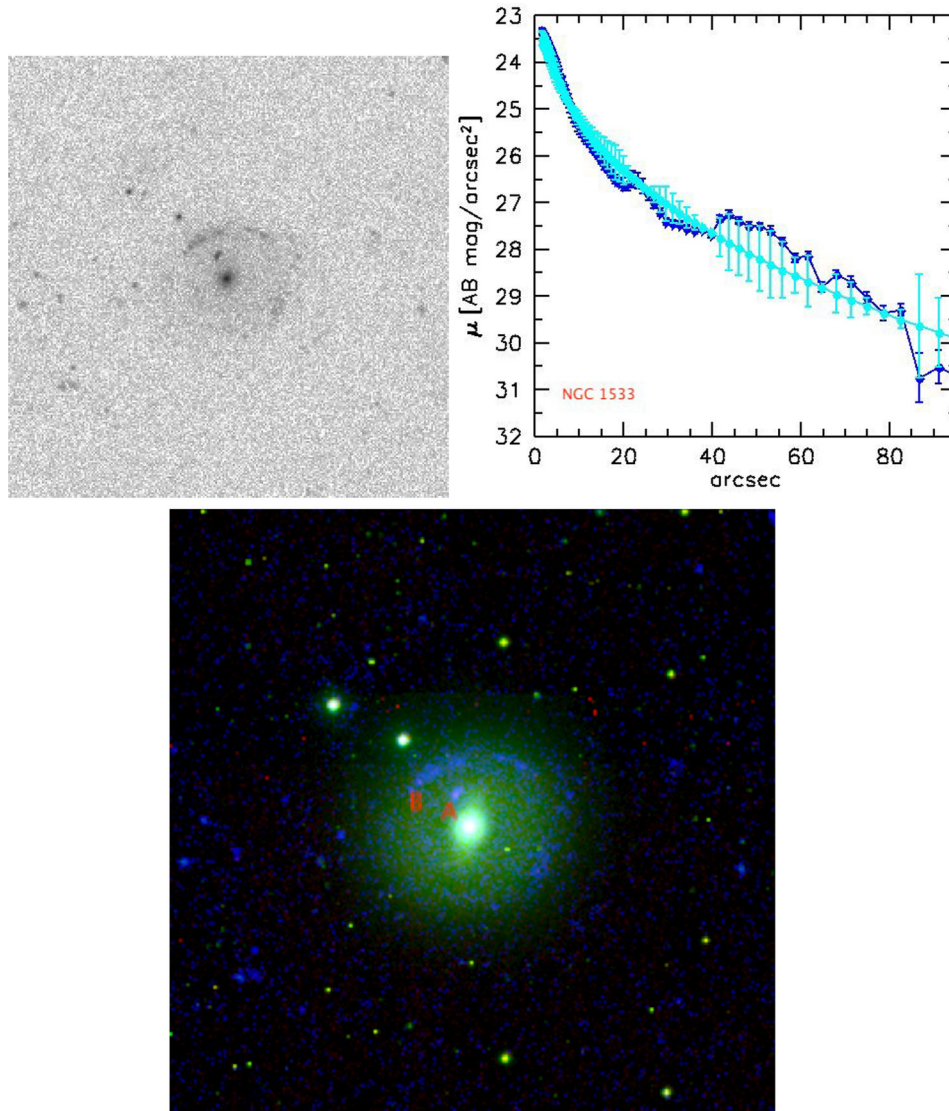


**Figure 5.** (Top: left panel) FUV image of NGC 1533. The image size is  $7' \times 7'$ . North on the top, east to the left. (Top: right panel) Surface brightness profile of NGC 1533 (blue dots) and single Sérsic law fit (cyan dots). The value of the Sérsic index is  $n = 2.64 \pm 0.06$ . (Bottom panel) As in Fig. 4, for NGC 1533. Labels A and B indicate H II regions in Rampazzo *et al.* (2020).

## 5. Results

In the following sections, we discuss the shape of the surface brightness profile and the morphology of the FUV emission.

### 5.1 Members surface photometry

IC 2038. In the top panels of Fig. 4, the FUV image and the luminosity profiles of IC 2038 and IC 2039 are shown.

IC 2038, classified as Sbc in optical by *HyperLeda*, does not show a bulge (see e.g. Rampazzo *et al.* 2020, their Fig. 3). The FUV emission appears clumpy in the centre of the galaxy, where H II regions are detected by Rampazzo *et al.* (2020), while an arm-like structure appears out the both sides of the galaxy body.

The FUV surface brightness profile is flat in the central  $\approx 20''$ . The best-fit to the entire profile has a Sérsic index of  $n = 0.81 \pm 0.09$  suggesting the galaxy is dominated by the disk. In the central  $\approx 25''$  there is an excess of luminosity with respect to the Sérsic law best fit, in correspondence to FUV clumps.



The FUV emission extends out to the optical size of the galaxy as shown by Fig. 4 and Fig. 1: there is no evidence of a XUV disk (Thilker 2008).

The average ellipticity,  $\langle\epsilon\rangle = 0.72 \pm 0.02$  and the average position angle  $\langle PA\rangle = 154.4^\circ \pm 4.6^\circ$ , compare well with values from optical bands,  $0.74 \pm 0.04$  and  $155.2^\circ$  respectively, from the *HyperLeda* catalog.

*IC 2039.* In FUV, IC 2039 is the faintest galaxy of the sub-structure (Fig. 2). We best-fit luminosity profile of IC 2039 (top right panel of Fig. 4) with a single Sérsic law with an index  $n = 1.45 \pm 0.18$  indicating that it is basically composed of a disc.

The average ellipticity is  $\langle\epsilon\rangle = 0.19 \pm 0.05$  and the position angle  $\langle PA\rangle = 104.1^\circ \pm 8.7^\circ$  to compare with optical values of  $0.15 \pm 0.07$  and  $124.3^\circ$  from *HyperLeda*.

*NGC 1533.* The galaxy, classified as E-S0 (*HyperLeda*) is known to have an outer ring and an inner bar, so Comerón *et al.* (2014) classified it as (RL)SB0<sup>0</sup>. However, in FUV this galaxy shows no signature of the bar. The presence of a FUV-bright outer ring was evidenced using *GALEX* by Marino *et al.* (2011b) both in NUV and FUV. UVIT clearly reveals a bright FUV spot at  $\approx 25''$  and the ring in the range  $39''$ – $81''$ , in agreement with Marino *et al.* (2011a) (their Table 1). Their presence causes a sudden jump of both  $\epsilon$  and PA. ELLIPSE provides  $\epsilon = 0.56 \pm 0.04$  and  $PA = 63^\circ$  within  $39''$  and  $\epsilon \approx 0.17 \pm 0.06$  and  $PA = 164^\circ$  outside the region of the ring up galaxy outskirts. The value of the ellipticity and PA provided by *HyperLeda* from optical bands are  $0.36 \pm 0.09$  and  $141.5^\circ$ .

The surface brightness profile (top right panel of Fig. 5) is best-fitted by a Sérsic law with index  $n = 2.64 \pm 0.06$  suggesting the presence of a disc. This value agrees with the UV Sérsic index of  $n = 2.76 \pm 0.10$  obtained from the

luminosity profile in the *Swift* W2 filter ( $\lambda_c = 2030 \text{ \AA}$ ) by Rampazzo *et al.* (2017).

## 5.2 FUV regions outside galaxies main body

To enhance the signal-to-noise ratio (S/N) in the galaxy outskirts and bring out any possible faint structures in the UV emission, we adopted the procedure outlined by Ebeling *et al.* (2006), called *ASMOOTH*. The only parameter required by the procedure is the desired minimal S/N,  $\tau_{\min}$ . For each individual pixel, the algorithm increases the smoothing scale until the S/N within the kernel reaches a specified input value. *ASMOOTH* suppresses very efficiently the noise while the signal, locally significant at the selected S/N level, is preserved on all scales. In the right and left panels of Fig. 6, the FUV image has been treated with *ASMOOTH* selecting a S/N above the background of  $\tau_{\min} = 1.5$  and  $\tau_{\min} = 2.0$ , respectively. The possible physical causes of the features that emerged using this procedure are discussed below.

Cattapan *et al.* (2019) (see their Fig. 7) superposed the emission of NGC 1533 in the W2 filter derived by Rampazzo *et al.* (2017) from *Swift*-UVOT observations to their wide field, deep *g*-band image obtained at VST (see Fig. 1). They found that the FUV ring of NGC 1533 is superposed to spiral-like residuals obtained after a model of the optical luminosity profile has been subtracted. The right panel of Fig. 6, the FUV image treated with *ASMOOTH* shows an arm-

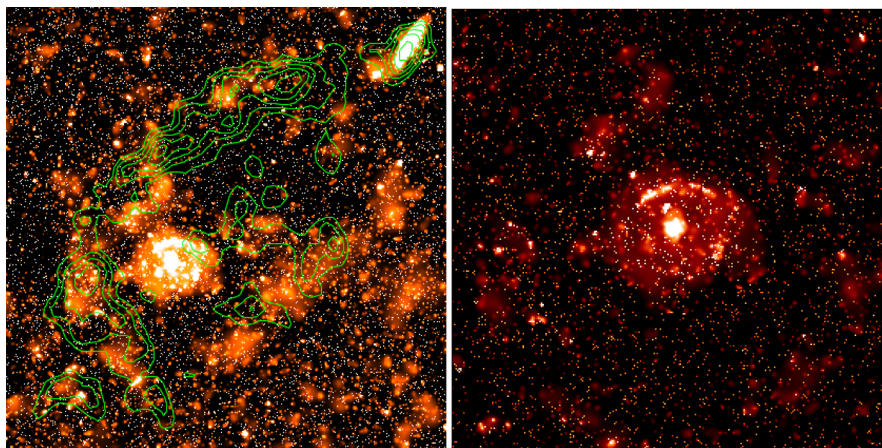


**Figure 6.** (Left panel) The H I contour levels from Ryan-Weber *et al.* (2004) at column densities  $2.5 \times 10^{20}$ ,  $2.8 \times 10^{20}$ ,  $3.1 \times 10^{20}$ ,  $3.5 \times 10^{20}$ ,  $3.9 \times 10^{20}$  and  $4.2 \times 10^{20}$  atoms  $\text{cm}^{-2}$  are superposed to the UVIT FUV image of the sub-structure after an adaptive smoothing (*ASMOOTH*) with a minimum S/N  $\tau_{\min} = 1.5$  (Ebeling *et al.* 2006) has been applied. The image size corresponds to Fig. 1. (Right panel) Zoom-in on NGC 1533 (field-of-view  $7' \times 7'$ ) showing the complex structure of the ring and an arm/like structure on the west side (*ASMOOTH* with a minimum S/N  $\tau_{\min} = 2$ ).

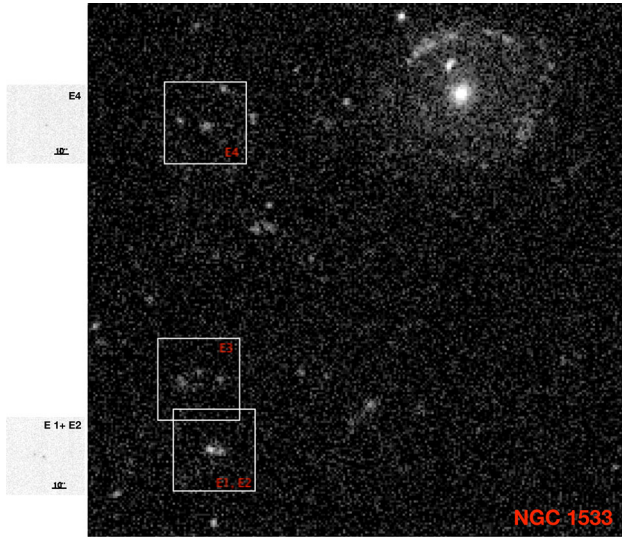


**Figure 7.** The south-east region of NGC 1533 observed in FUV by UVIT. Three boxes of  $60'' \times 60''$  in the FUV image enclose the regions identified as J0409-56 E1 + E2, E3, E4 by Werk *et al.* (2010) on *GALEX* in which they found H $\alpha$  sources. The two areas, showed as sub-panels on the right of the FUV image, mark the position of H II regions, at the same redshift of the galaxy, detected by Rampazzo *et al.* (2020) via H $\alpha$  + [N II] observations. The centres of the regions in Rampazzo *et al.* (2020) correspond to the following coordinates 04 10 13.5–56 11 36 (J2000) and 04 10 10.66–56 07 27.99 (J2000) and overlap with region E1 + E2 and E4 in Werk *et al.* (2010), respectively.

like structure is emerging also in FUV outside the ring in the west side.

In the left panel of Fig. 6, we overplot the H I emission isophotes from Ryan-Weber *et al.* (2004). While the center of NGC 1533, in particular the ring, is devoid of H I the large scale structure of H I seems to corresponds to the faint extended FUV emission derived using *ASMOOTH*. The ATCA H I observations by Ryan-Weber *et al.* (2004) extended over an area at least  $\approx 5'$  to west (partly covered by Fig. 6). They do not detect any H I to the west within their detection limit. Some FUV emission regions above  $\tau_{\min} = 1.5$  are still visible in that area. The presence of this FUV emission would be consistent with the N-body SPH numerical simulations by Ryan-Weber *et al.* (2003) describing the H I ring around NGC 1533 as the remnant of a tidally destroyed galaxy (see Section 6.2).

Figure 7 shows the outer FUV emission regions of NGC 1533, investigated by Werk *et al.* (2008, 2010) in the first systematic search for outlying H II regions, as part of a sample of 96 emission-line point sources

(referred to as ELdots-emission-line dots) derived from the NOAO Survey for Ionization in Neutral Gas Galaxies (SINGG). Such regions, selected from *GALEX* FUV, are indicated in the above paper as J0409-56 E1, E2, E3 and E4. Rampazzo *et al.* (2020) inspected also the corresponding areas looking for H II regions in their frames. Those found are shown right panels of Fig. 7 and indicated as E1+E2 and E4. Rampazzo *et al.* did not detect H II regions in the zone indicated as E3. Indeed, Werk *et al.* (2010) found that their targets span over a large range in H $\alpha$  luminosities which correspond to a few O stars in most of the nearby cases. Werk *et al.* (2010) emphasized that often FUV sources are mixed to unresolved dwarf satellite companions and background galaxies. Outer H II regions of NGC 1533 may be linked to the strong interacting phase suggested by Cattapan *et al.* (2019) and well imaged in their Fig. 6. H II regions detected and their embedded young stars are definitely correlated with H I as their velocities are the same (see Section 6.2).

## 6. Discussion

The NGC 1533 sub-structure in the Dorado group has been recently studied by Cattapan *et al.* (2019) in *g* and *r* SDSS-bands and by Rampazzo *et al.* (2020) in H $\alpha$ + [N II]. This substructure with a heliocentric velocity  $V_{\text{hel}} \approx 764 \text{ km s}^{-1}$  is still evolving separately from the Dorado core, the compact group SCG 0414-5559 (Iovino 2002), with  $V_{\text{hel}} \approx 1230 \text{ km s}^{-1}$ . Both IC 2038/IC 2039 and NGC 1533 show several interaction signatures as described in Cattapan *et al.* (2019) (see their Fig. 6). Their environment is H I rich (Ryan-Weber *et al.* 2003; Kilborn *et al.* 2009). The above studies suggest a common evolutionary picture of the galaxies members of the NGC 1533 sub-structure.

### 6.1 FUV and evolution of member galaxies

Mazzei *et al.* (2014a, 2019) and references therein, using smoothed particle hydrodynamic simulations with chemo-photometric implementation (SPH-CPI), investigated the evolutionary path of NGC 1533, the dominant member of the sub-structure.

From a large grid of simulations of galaxy encounters and mergers, starting from triaxial halos of gas and dark matter, a simulation matching the global

properties of this SB0 galaxy (absolute B mag, SED, luminosity profile, morphology at different wavelengths and kinematics properties) has been single out. According to this study NGC 1533 is the result of a major merging occurred at  $z = 2.3$ . 40% of its current mass is assembled before  $z = 1$ .

The FUV bright ring has been one of the morphological features used to single out the simulation from the SPH-CPI grid. The ring is, indeed, well reproduced by the selected simulation as the result of a resonance that appeared when the galaxy is 8 Gyr old and is maintained up to now. The simulation showed the path of NGC 1533 in the (NUV- $r$ ) vs.  $M_r$  color-magnitude diagram. NGC 1533 is 13.7 Gyr old, that it spends as follows. It lies on the blue cloud for 7.2 Gyr, from there it takes about 0.9 Gyr to reach the green valley that will cross reaching the red sequence in 1.6 Gyr, finally it gets its current position on the red sequence after additional 4 Gyr.

The evolution of the pair IC 2038/IC 2039 has not been studied yet. The pair badly lack a detailed kinematic study in order to constrain the SPH-CPI grid of simulations. As relevant examples in this context, we mention the SPH-CPI studies of the pair NGC 454 by and of the false pair NGC 3447/NGC 3447A by Plana *et al.* (2017a, b), Mazzei *et al.* (2018).

## 6.2 FUV and SF regions

The FUV emission is a short scale ( $\approx 10^7$  years) SF indicator. Therefore it can be associated to a measure of the SF obtained from H $\alpha$  ( $\approx 10^6$  years) (see Kennicutt & Evans 2009). Next sections will focus on SF regions and SFR estimates from H $\alpha$  and FUV.

The FUV emission of IC 2038 is more extended than the area where H II regions are found. Indeed, the FUV emission covers the entire galaxy seen in the continuum (optical) image (bottom panel of Fig. 4). The FUV emission is also present in the inner regions of IC 2039 (Fig. 4). However, no H II regions have been detected in this E-S0 by Rampazzo *et al.* (2020).

At odds, in NGC 1533 H II regions are found in two small complexes by Rampazzo *et al.* (2020) and labelled as A and B in Fig. 5. In this galaxy the FUV emission concentrates in the ring and a bright FUV spot, that includes the above H II regions.

We revealed in this paper a faint FUV emission (Fig. 6) associated to a complex H I structures composed of two major arcs one north west and a second south east (Ryan-Weber *et al.* 2004). No optical counterparts are connected with these arcs. Faint H II

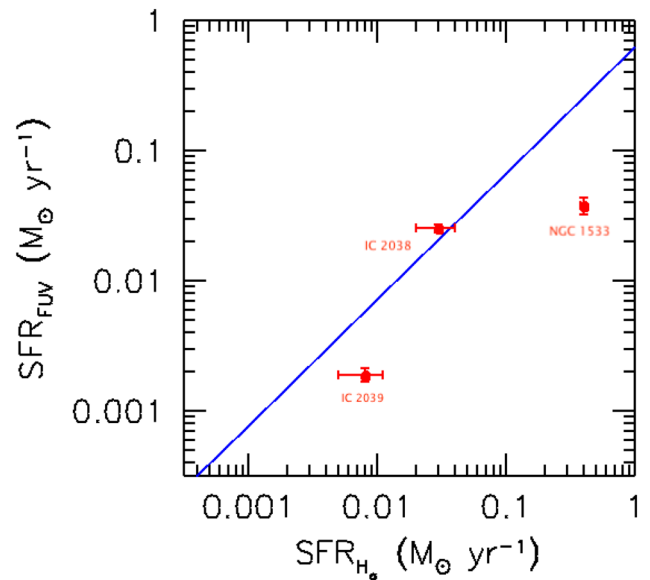


**Figure 8.** Comparison between the SFR computed from H $\alpha$  and FUV emission without accounting for internal extinction. The blue solid line show the relation found by Lee *et al.* 2009 (see text).

regions are found south east of NGC 1533 (Werk *et al.* 2008, 2010; Rampazzo *et al.* 2020) and are correlated to the H I envelope. In particular regions indicated in Fig. 7 as E1–E2 have a recession velocity of 831 and 846  $\text{km s}^{-1}$  (another region indicated E5 by Ryan-Weber *et al.* 2004, see their Fig. 2) has a recession velocity of 901  $\text{km s}^{-1}$ ). With these recession velocities H II regions are compatible with being associated to NGC 1553 sub-structure (see Table 1) and with the H I structure as well.

Concerning the origin of the H I clouds around NGC 1533, Ryan-Weber *et al.* (2003) suggested that it could be the merger remnant of a tidally destroyed galaxy. Ryan-Weber *et al.* (2004) noticed that the H I gas in the south east cloud has velocity dispersion up to 30  $\text{km s}^{-1}$  and velocity gradient in the range 7–50  $\text{km s}^{-1} \text{ kpc}^{-1}$ . These conditions makes this site unlikely for SF since the latter usually requires the gas to have a low velocity dispersion in order to collapse.

We conclude that the H I arcs detected by Ryan-Weber *et al.* (2004), the correspondent faint FUV structure revealed in this paper in addition to the optical evidence of faint tails and arcs shown by the (Cattapan *et al.* 2019) deep surface photometry are indication that galaxy–galaxy encounters, leading to galaxy tidal disruption (Ryan-Weber *et al.* 2003) and merging events (Mazzei *et al.* 2019) are the drivers of

the complex evolution within the NGC 1533 sub-structure.

### 6.3 SFR from FUV integrated galaxy luminosity

In this section, we compare the SFR for our three targets as derived by H $\alpha$  emission (Rampazzo *et al.* 2020) with that by the integrated FUV emission in this paper.

We follow the recipes of Lee *et al.* (2009, their equation (3)) to compute the SFR for FUV:

$$\text{SFR} (M_{\odot} \text{ yr}^{-1}) = 1.4 \times 10^{-28} L_{\text{FUV}} (\text{ergs}^{-1} \text{ Hz}^{-1}). \quad (1)$$

Lee *et al.* (2009) found the following relation when the effects of internal dust attenuation are not included:

$$\log(\text{SFR}(\text{FUV})) = 0.79 \log(\text{SFR}(\text{H}\alpha)) - 0.20. \quad (2)$$

This is highlighted by a solid blue line in Fig. 8. Lee *et al.* (2009) noticed that H $\alpha$  and FUV SFRs agree to within factor of  $\approx 2$  for all galaxies with  $\text{SFR} \geq 0.01 M_{\odot} \text{ yr}^{-1}$ .

The SFR of IC 2038, the only LTG in the sub-structure, does not deviate from the Lee *et al.* (2009) relation. However, according to Rampazzo *et al.* (2020) the SFR of IC 2038 estimated from H $\alpha$  is below the average for its morphological class estimated by James *et al.* (2004).

The SFR of the two ETGs, IC 2039 and NGC 1533 seems to deviate from the Lee *et al.* (2009) relation, suggesting a higher SFR from H $\alpha$  than from UV. This point is quite surprising given that UV stars trace SFR with a time scale longer than H $\alpha$  and the activity of SF is residual for ETGs.

Figure 2 and Table 2 in Lee *et al.* (2009) showed the trend of the ratio  $\log[\text{SFR}(\text{H}\alpha)/\text{SFR}(\text{FUV})]$  as a function of the B-band galaxy absolute magnitude. At the distance of Dorado, the absolute B magnitude of NGC 1533 and IC 2039 is  $M_B = -19.52$  and  $-16.3$ , respectively. At these magnitudes, Lee *et al.* (2009) reported the average values of  $\log[\text{SFR}(\text{H}\alpha)/\text{SFR}(\text{FUV})] \approx -0.10 \pm 0.36$  ( $1\sigma$ ) and  $\log[\text{SFR}(\text{H}\alpha)/\text{SFR}(\text{FUV})] \approx -0.12 \pm 0.18$ . Our measured values are  $\log[\text{SFR}(\text{H}\alpha)/\text{SFR}(\text{FUV})] = 1.02$  and  $\log[\text{SFR}(\text{H}\alpha)/\text{SFR}(\text{FUV})] = 0.6$  for NGC 1533 and IC 2039, respectively. However, the bottom panel of Fig. 2 in Lee *et al.* (2009) showed discrepant cases of galaxies, with values of  $\log[\text{SFR}(\text{H}\alpha)/\text{SFR}(\text{FUV})]$  similar to ours. Investigating

the SF properties in the Local Volume of Galaxies with H $\alpha$  and FUV fluxes, Karachentsev and Kaisina (2013) provided a  $\log[\text{SFR}(\text{H}\alpha)/\text{SFR}(\text{FUV})] = 1$  for NGC 1533, in well agreement with our value.

We plan to further explore the comparison of SFR from H $\alpha$  and FUV using the entire UVIT data-set of the Dorado backbone, considering extinction effects in more detail than in Lee *et al.* (2009) assumptions (Rampazzo *et al.* in preparation). The SPH chemophotometric simulation of NGC 1533 by Mazzei *et al.* (2019) provided an estimate of the internal galaxy extinction. We will use also such estimates.

## 7. Summary and conclusion

We performed with UVIT a FUV photometric study of a substructure of the Dorado group of galaxies that includes three galaxies: the mixed morphology pair IC 2038 (Sbc)/2039 (E-S0) and NGC 1533. We derived their luminosity profiles and discussed their FUV morphologies.

We found the following results:

- The shape of the FUV luminosity profile indicates the presence of a disc in all three galaxies. The presence of disc suggests that dissipative mechanisms have been at work.
- In IC 2038, the FUV emission is detected out to the optical size for IC 2038, further out than the H II regions system detected by Rampazzo *et al.* (2020). There is no evidence of a XUV disk (Thilker 2008).
- In IC 2039, the FUV emission is detected in the inner regions where no H II regions have been detected by Rampazzo *et al.* (2020).
- In NGC 1533, the FUV emission is more extended than the system of H II regions detected by Rampazzo *et al.* (2020). The extended FUV emitting regions likely correspond to outer arm-like structures detected at different wavelengths (Marino *et al.* 2011a; Rampazzo *et al.* 2017; Cattapan *et al.* 2019).
- We reveal a faint FUV emission, just above the local background noise, reminiscent of the wide H I structure detected by Ryan-Weber *et al.* (2004). In the east and south east regions of this FUV emission lurk few H II regions highlighted by Werk *et al.* (2008, 2010) and Rampazzo *et al.* (2020) with the same redshift as the H I structure (Ryan-Weber *et al.* 2004) and of the NGC 1533 sub-structure as well.

- We derive the SFR from the FUV luminosity and we compare the results with SFR, following the Lee *et al.* (2009) recipe, with SFR from H $\alpha$  by Rampazzo *et al.* (2020). The SFR for IC 2038 only agrees with Lee *et al.* (2009) expected ratio between FUV and H $\alpha$  derived values. At odds, our measure of the SFR H $\alpha$ /FUV for NGC 1533 well agrees with that found by Karachentsev and Kaisina (2013).

Lee *et al.* (2009) SFR(FUV)–SFR (H $\alpha$ ) relation does not account for internal dust effects. Such relation will be investigated further in the analysis of our UVIT FUV observations of the whole galaxy group.

In a forthcoming paper, we will analyze the central part of Dorado, the compact group SGC 0414-5559 Iovino (2002), composed of NGC 1553, NGC 1549, NGC 1546 and IC 2058 plus the dwarf galaxy PGC 75125. The study of the SBc galaxy NGC 1536 and of the mixed pair NGC 1596/NGC 1602 (S0+Irr), part of the A07 program but non yet observed, will complete our study of the Dorado backbone with UVIT.

## Acknowledgements

This publication uses the data from the AstroSat mission of the Indian Space Research Organisation (ISRO), archived at the Indian Space Science Data Centre (ISSDC). This publication uses UVIT data processed by the payload operations centre at IIA. The UVIT is built in collaboration between IIA, IUCAA, TIFR, ISRO and CSA.

## References

- Barnes J. E. 2002, MNRAS, 333, 481  
 Bender R., Döbereiner S., Möllenhoff C. 1988, A&AS, 74, 385  
 Boselli A., Gavazzi G. 2006, PASP, 118, 517  
 Boselli A., Gavazzi G. 2014, A&A Review, 22, 74  
 Bureau M., Carignan C. 2002, AJ, 123, 1316  
 Capaccioli M., Spavone M., Grado A. *et al.* 2015, A&A, 581, A10  
 Cattapan A., Spavone M., Iodice E. *et al.* 2019, ApJ, 874, 130  
 Chung A., Koribalski B., Bureau M., van Gorkom J. H. 2006, MNRAS, 370, 1565  
 Comerón S., Salo H., Laurikainen E. *et al.* 2014, A&A, 562, A121  
 de Vaucouleurs G. 1953, MNRAS, 113, 134.  
 Di Matteo T. 2015, in: IAU General Assembly, vol. 29, 2257908  
 Domingue D. L., Sulentic J. W., Xu C. *et al.* 2003, AJ, 125, 555  
 Ebeling H., White D. A., Rangarajan F. V. N. 2006, MNRAS, 368, 65  
 Firth P., Evstigneeva E. A., Jones J. B. *et al.* 2006, MNRAS, 372, 1865  
 Freeman K. C. 1970, ApJ, 160, 811  
 Gavazzi G., Consolandi G., Pedraglio S. *et al.* 2018, A&A, 611, A28  
 Iovino A. 2002, AJ, 124, 2471  
 Jedrzejewski R. I. 1987, MNRAS, 226, 747  
 James P. A., Shane N. S., Beckman J. E. *et al.* 2004, A&A, 414, 23  
 Jeong H., Yi S. K., Bureau M. *et al.* 2009, MNRAS, 398, 2028  
 Karachentsev I. D., Kaisina E. I. 2013, AJ, 146, 46.  
 Kantharia N. G., Ananthakrishnan S., Nityananda R., Hota A. 2005, A&A, 435, 483  
 Keel W. C. 2004, AJ, 127, 1325  
 Kennicutt R. C., Evans N. J. 2009, Ann. Rev. A&A, 50, 531  
 Kilborn V. A., Koribalski B. S., Forbes D. A. *et al.* 2005, MNRAS, 356, 77  
 Kilborn V. A., Forbes D. A., Barnes D. G. *et al.* 2009, MNRAS, 400, 1962  
 Kourkchi E., Tully R. B. 2017, ApJ, 843, 16  
 Kumar A., Ghosh S. K., Hutchings J. *et al.* 2012, Proc. SPIE, 8443, 84431N  
 Lee J. C., Gil de Paz A., Tremonti C. *et al.* 2009, ApJ, 706, 599  
 Malin D. F., Carter D. 1983, ApJ, 274, 534  
 Marino A., Bianchi L., Rampazzo R. *et al.* 2010, A&A, 511, A29  
 Marino A., Bianchi L., Rampazzo R. *et al.* 2011a, ApJ, 736, 154  
 Marino A., Rampazzo R., Bianchi L. *et al.* 2011b, MNRAS, 411, 311  
 Marino A., Plana H., Rampazzo R. *et al.* 2013, MNRAS, 428, 476  
 Marino A., Mazzei P., Rampazzo R., Bianchi L. 2016, MNRAS, 459, 2212  
 Martin D. C., Fanson J., Schiminovich D. *et al.* 2005, ApJ, 619, L1  
 Mazzei P., Marino A., Rampazzo R., Galletta G., Bettoni D. 2014a, Adv. Space Res., 53, 950  
 Mazzei P., Marino A., Rampazzo R. 2014b, ApJ, 782, 53  
 Mazzei P., Marino A., Rampazzo R. *et al.* 2018, A&A, 610, A8  
 Mazzei P., Rampazzo R., Marino A., Trinchieri G., Uslenghi M., Wolter A. 2019, ApJ, 885, 165  
 Morrissey P., Conrow T., Barlow T. A. *et al.* 2007, ApJS, 173, 682  
 Plana H., Rampazzo R., Mazzei P. 2017, MNRAS, 472, 3074.  
 Plana H, Rampazzo R., Mazzei P. *et al.* 2017, MNRAS, 472, 3074  
 Postma J., Hutchings J. B., Leahy D. 2011, PASP, 123, 833

- Postma J., Leahy D. 2017, *PASP*, 129, 981  
Postma J., Leahy D. 2020, *PASP*, 132, 1011  
Ramatsoku M., Serra P., Poggianti B. M. *et al.* 2019, *MNRAS*, 487, 4580  
Rampazzo R., Mazzei P., Marino A. *et al.* 2017 *A&A*, 602, A97  
Rampazzo R., Mazzei P., Marino A. *et al.* 2018, *Ap&SS*, 363, 80  
Rampazzo R., Ciroi S., Mazzei P. *et al.* 2020, *A&A*, 643, A176  
Ryan-Weber E. V., Meurer G. R., Freeman K. C. *et al.* 2004, *AJ*, 127, 143  
Ryan-Weber E., Webster R., Bekki K. 2003, *The IGM/Galaxy Connection: The Distribution of Baryons at  $z = 0$* , *ASSL Conference Proceedings*, vol. 281, edited by Jessica L. Rosenberg and Mary E. Putman, ISBN: 1-4020-1289-6, Kluwer Academic Publishers, Dordrecht, p. 223  
Salim S., Rich R. M., Charlot S. *et al.* 2007, *ApJS*, 173, 267  
Schawinski K., Kaviraj S., Khochfar S. *et al.* 2007, *The Astrophys. J. Suppl. Series*, 173, 512  
Sérsic J. L. 1963, *Jan, Boletin de la Asociacion Argentina de Astronomia La Plata Argentina*, 6, 41  
Tandon S. N., Subramaniam A., Girish V. *et al.* 2017, *AJ*, 154, 128  
Tandon S. N., Postma J., Joseph P. *et al.* 2020, *AJ*, 159, 158  
Thilker D. 2008, *Astrophys. Space Sci. Proc.*, *Galaxies in the Local Volume*, edited by Koribalski B. S., Jerjen H., 109  
Toomre A., Toomre J. 1972, *ApJ*, 178, 623  
Werk J. K., Putman M. E., Meurer G. R. *et al.* 2008, *ApJ*, 678, 888  
Werk J. K., Putman M. E., Meurer G. R. *et al.* 2010, *AJ*, 139, 279